Infrastructure network component vulnerability to damage from the 2015 Illapel tsunami, Coquimbo, Chile

James Hilton Williams (j.williams@canterbury.ac.nz)
University of Canterbury School of Earth and Environment https://orcid.org/0000-0002-7564-0032
Ryan Paulik
NIWA: National Institute of Water and Atmospheric Research
Rafael Aránguiz
Universidad Catolica de La Santisima Concepcion
Alec Wild
NIWA: National Institute of Water and Atmospheric Research

Research Article

Keywords: Tsunami, critical infrastructure, damage, fragility curves, Chile

Posted Date: February 10th, 2022

DOI: https://doi.org/10.21203/rs.3.rs-1104603/v1

Abstract

This study presents critical infrastructure network component vulnerability in the 2015 Illapel tsunami at Coquimbo, Chile. We analyse road and utility pole vulnerability to physical damage based on modelled tsunami hazard intensity (depth, velocity and hydrodynamic force) and network component characteristics. A Random Forest Model and Spearman's Rank correlation test are applied to analyse variable importance and monotonic relationships between tsunami hazards and network component attributes with damage levels. These models and tests revealed scour and debris impacts are highly important and strongly correlated with road and utility pole damage levels, while flow depth correlates higher with damage levels relative to flow velocity and hydrodynamic force. A cumulative link model methodology is used to develop fragility curves, The fragility curves in response to flow depth revealed roads have higher vulnerability than those analysed in previous tsunami events (e.g. 2011 Tohoku, 2018 Sulawesi, 2015 Illapel Tsunami), while utility poles demonstrate lower vulnerability. Although we identify flow depth as the hydrodynamic hazard intensity metric of highest importance for causing road and utility pole physical damage, fragility curves representing multiple hazard intensities provides a holistic curve suite for analysing infrastructure network damage and disruption from future tsunami events.

1. Introduction

Critical infrastructure networks are crucial to the everyday functioning of society. Since the 2004 Indian Ocean tsunami, widespread damage to network components have been observed (Ballantyne, 2006; Edwards, 2006; Evans and McGhie, 2011; Fritz et al., 2011; Goff et al., 2006; Maruyama and Itagaki, 2017; Palliyaguru and Amaratunga, 2008; Paulik et al., 2021; Scawthorn et al., 2006; Tang et al., 2006). Analysing component damage in response to tsunami hazard is required for establishing context specific vulnerability models for network components. These models are critical for quantifying the physical damage to network components, and the service disruption to networks, from tsunami events.

Used approaches include the development of tsunami vulnerability and fragility curves, which define the relationship between network component damage level and hazard intensity (e.g. tsunami flow depth; Koshimura et al., 2009). Vulnerability curves derive a continuous loss index or ratio as intensity increases for the given hazard intensity measure (HIM), whereas fragility curves provide the probability of exceeding different limit states (e.g. physical damage) for the given HIM (Koshimura et al., 2009). Tsunami fragility curves are typically developed from empirical component attribute and impact data, and empirical or numerical hazard data for a specific event. The data are, therefore, representative of the events' hazard characteristics and local network component construction standards. The synthesised curves may, or may not, be applicable to other settings, so it has been identified as an important priority of tsunami risk science to undertake post-event tsunami hazard and impact surveys that contribute towards progressively more comprehensive global datasets and inform increasingly effective disaster risk assessment. Tsunami vulnerability assessment has largely focused on building damage (Tarbotton et al., 2015), and there is now a need to focus on other elements of the built environment including infrastructure networks.

Tsunami fragility curves commonly rely on relatively large samples of empirical or modelled impact damage data, yet such quantitative empirical data for infrastructure vulnerability are rare and have only recently been a focus of post-event impact assessment (MLIT, 2012; Paulik et al., 2019, 2021) and physical modelling studies (C Chen and Melville, 2015; Cheng Chen et al., 2017, 2018; Rossetto et al., 2014). For infrastructure networks, transportation components, namely roads, bridges, utility poles and port structures, have been previously analysed for fragility function development from empirical field surveys and physical modelling (Chua et al., 2020; Eguchi et al., 2013; Kawashima and Buckle, 2013; Koks et al., 2019; Maruyama and Itagaki, 2017; Shoji and Moriyama, 2007; Williams, et al., 2020b; Williams, et al., 2020a). However, the relative importance of network component attribute characteristics influencing tsunami damage is understudied. These previous fragility studies typically apply tsunami flow depth as the HIM, as it has a strong correlation with impact and can be measured post-event. Empirical tsunami flow depth data can be used for interpolated hazard models (e.g. Williams, et al., 2020b; Williams, et al., 2020a) and/or to refine and validate numerical hazard models (e.g. Aránguiz et al., 2018; Heidarzadeh et al., 2015; Jamelot et al., 2019). However tsunami hazard and impact studies to date are almost unanimous in that no single HIM can fully encapsulate the characteristics of tsunami impacts (Bojorquez et al., 2012; Gehl and D'Ayala, 2015; Joshua Macabuag et al., 2016). Furthermore, a number of studies recommend the development of tsunami fragility curves for infrastructure network components that consider tsunami flow velocity and hydrodynamic force (e.g. Williams, et al., 2020b and Williams, et al., 2020a) among other HIMs.

The present study has two main objectives. Analyse and discuss the factors causing damage to roads and utility poles, using empirical data collected from Coquimbo (Chile) after the 2015 Illapel tsunami. Secondly, develop fragility curves on the conditional probability of physical damage levels for these network components in response to tsunami flow depth, flow velocity and hydrodynamic force. To that affect, this paper provides an overview of the case-study event (Section 2), methodology (Section 3), including the empirical damage dataset (Section 3.1), tsunami hazard data (Section 3.2), variable testing for feature importance and correlation (Section 3.3) and fragility function development (Section 3.4) using a cumulative link model method. The results of the variable importance and correlation tests are presented (Section 4.1), followed by the tsunami fragility curves (Section 4.2) for roads (Section 4.2.1) and utility poles (Section 4.2.2). A discussion of the results (Section 5), including and their potential limitations are then followed by a summary of the study (Section 6).

2. Case Study Event

The 16 September 2015 Illapel tsunami occurred following a large earthquake that struck off the central Chile coast (Fig. 1). The most impacted regions were between La Serena and Concón, Valparaíso (ONEMI, 2015). The event motivated several post-event field surveys, with teams measuring and recording tsunami hazard characteristics and damage along a 700 km stretch of coastline from Chañaral to Concón (Aránguiz et al., 2016; Tomita et al., 2016). Horizontal flow and run-up measurements were mostly taken between La Serena and Los Vilos (Aránguiz et al., 2016) with building, critical infrastructure and environmental (i.e. wetland) damage observed in Coquimbo and Los Vilos (Aránguiz et al., 2016;

Contreras-López et al., 2016; Paulik et al., 2021). In Coquimbo (pop. 209,684), tsunami wave heights reached 4.75 m at the Port tide gauge, causing a maximum run-up height of 6.4 m (Aránguiz et al., 2016; Contreras-López et al., 2016). Critical infrastructure network damage and disruption were cited in immediate tsunami damage reports (ONEMI, 2015), however, network component damage investigations were not a primary focus of national-led post-event surveys.

Post-tsunami surveys prior to this event have mainly focused on systematic building damage assessments opposed to component damage sustained by transport, energy, water and telecommunications networks. Empirical information on tsunami hazard intensity, critical infrastructure component attributes and damage level are critical for analysing the fragility of individual network components. Critical infrastructure network component fragility curves can support investigations of potential service disruption to single or multiple networks affected by tsunamis. Previous studies on this event have focused on surveying the hazard to determine tsunami source characteristics (Aránguiz et al., 2016), damage observations (Aránguiz et al., 2016; Contreras-López et al., 2016; Paulik et al., 2021), interpolated and simulated hazard models (Aránguiz et al., 2018; Klapp et al., 2020) and vulnerability models for buildings (Aránguiz et al., 2018) and road network components (Williams et al., 2020a). The data used to develop fragility curves in the current study represent road and utility pole damage levels (Paulik et al., 2021; Table 1), interpolated tsunami flow depths (Williams et al., 2020a) and numerical hydrodynamic tsunami models (Aránguiz et al., 2018; Fig. 2) for Coquimbo.

3. Methodology

3.1 Empirical damage data

Paulik et al. (2021) recorded tsunami flow depths and classified building, road and utility pole (among others) attributes and damage levels (Table 1) in Coquimbo following the 2015 Illapel tsunami. Damage level (DL) classifications for roads and utility poles were categorised using an ordinal scale ranging from DL0 (No damage) to DL3 (Complete damage). The scheme applies a four-state damage level division (Table 3) tsunami vulnerability analysis and damage mapping applications for critical infrastructure network components. Roads and utility pole attribute information applied in the present study is presented in Table 2, along with the tsunami hazard characteristics. Road observation points were converted into linear features by Williams et al. (2020a) to represent attribute and damage levels for road network components exposed to tsunami hazards. In total 24 km of roads and 897 utility poles are recorded in the study area (Table 1).

Table 1
Summary of field data collected for tsunami hazard and damage for road and utility poles located in the study area

(modified from Paulik et al 2021)

Variable	Attribute	DL0	DL1	DL2	DL3
Road material	Concrete	10.1 km	0.8 km	0.5 km	0 km
	Asphalt	11 km	0.5 km	0 km	1.1 km
	Unsealed	0 km	0.2 km	0 km	0.06 km
Utility Pole Construction Material	Concrete	372	7	5	8
	Steel	287	69	10	98
	Timber	27	5	3	6

Table 2
Tsunami hazard and network component characteristics

Characteristic	Variable	Data type	Attributes or Description
Hydrodynamic tsunami hazard	IDmax	Decimal	Maximum interpolated flow depth (m)
	Dmax	Decimal	Maximum simulated flow depth (m)
	Vmax	Decimal	Maximum simulated flow velocity (m/s)
	Fmax	Decimal	Maximum simulated hydrodynamic force (kN/m)
Non-hydrodynamic tsunami hazard	Scour	Boolean	Presence of scour (yes/no)
	Debris impact	Boolean	Presence of debris impact damage (yes/no)
Roads	Road surface	Text	concrete, asphalt, unsealed
	Capacity	Text	Collector, local
	Lanes	Integer	Number of carriageway lanes
	Culvert	Boolean	Presence of culvert beneath road (yes/no)
	Distance from a coastline	Decimal	Distance from nearest coastline (m)
Utility Poles	Pole material	Text	Concrete, steel, timber
	Pole height	Text	<5 m, >5 m
	Distance from a coastline	Decimal	Distance from nearest coastline (m)

Table 3
Damage level descriptions for network components in Coquimbo survey area

(modified from Paulik et al. (2021)).

Component	DL0	DL1	DL2	DL3
	No Damage	Partial Damage, Repairable	Partial Damage, Unrepairable	Complete Damage
Road	-	Minor damage to road surface, all lanes passable with caution	Major damage to one lane. One lane impassable	Major damage to whole carriageway, all lanes impassable
Utility Pole	-	Scour or minor damage at base, pole in place	Buckling of pole, damage to pole base/foundation	Pole bent, snapped or sheared from base/foundations

3.2 Tsunami hazard models

Hydrodynamic tsunami hazard characteristics (Table 2) are estimated at roads and utility poles locations using interpolated (Williams et al., 2020a) and simulated (Aránguiz et al., 2018) representations of the 2015 Illapel tsunami. The single hazard intensity metric (HIM), an assumed maximum tsunami flow depth, is represented by the interpolated (spline method) water surface created by Williams et al. (2020a). Aránguiz et al. (2018) developed hydrodynamic tsunami models for the study area by means of numerical simulation. The authors applied the Non-hydrostatic Evolution of Ocean WAVEs (NEOWAVE) model with five nested grids at a maximum grid resolution of 10 m, and the Li et al. (2016) earthquake source model, to quantify maximum flow depth (m), flow velocity (m/s) and hydrodynamic force (kN/m) for the main urban centre of tsunami exposed Coquimbo (Fig. 2). The four tsunami HIMs represented by these datasets were spatially sampled at road and utility pole feature locations for vulnerability analysis and fragility curve development.

3.3 Variable testing for feature importance and correlation

Determining the importance and relationships between variables leading to tsunami damage is critical for understanding the dependencies and uncertainties of tsunami vulnerability models. The damage sample was analysed using a random forest model (RFM) to identify non-linear and non-monotonic variable dependence and Spearman's rank-order correlation tests (SRC) to detect monotonic relationships. Tsunami hazard (hydrodynamic and non-hydrodynamic) and network component attribute predictor variables (from Table 2) were applied in each model. Road and utility pole damage levels were the dependant variables in RFM to identify feature importance for damage.

The damage data sample was processed for RFM and SRC tests using the scikit-learn 0.24.2 package for Python. Eighteen tsunami hazard and network component attribute predictor variables (i.e. 4

hydrodynamic, 2 non-hydrodynamic, 7 road and 6 utility pole variables) were selected and binary-coded if required prior to processing (Table 2). The RFM applied 1000 trees with 4 random variables per split for both road and utility pole components, based on the square root of the predictor variable count. The number of trees represents the default setting of the algorithm. Variable feature importance is derived from RFM by mean decrease Gini, with loss in model performance when permuting the feature values indicating importance (Breiman, 2001). Here, the higher mean decrease Gini is an indicator of higher predictor variable importance for flood damage. The SRC test was then applied to analyse their feature importance with predictor variables applied in the RFM. The correlation test determines the strength and direction (i.e. positive or negative) of monotonic relationships between two predictor variables. The correlation significance (*p* value) for variable combinations was reported to indicate the relative significance of predictor variable relationships.

3.4 Fragility curve development

Fragility curves provide a probabilistic relationship between tsunami HIMs, and infrastructure component damage. In this study, synthesised tsunami HIM and network component attribute information are applied in cumulative link models (CLM) to construct fragility curves (Lallemant et al., 2015; J Macabuag et al., 2016). Previous empirical fragility curves for Coquimbo roads (Williams et al., 2020a) applied ordinary least square regression methods (OLS). However, this method can result in overlapping fragility curves that are not representative of network component damage characteristics (Williams et al., 2020b). CLMs are an extension of general link models (GLMs), which use the ordinality of damage levels, where increasing damage levels correspond to increasing damage severity (Charvet et al., 2014). Damage level ordering allows cumulative probabilities to be calculated for each damage level simultaneously. Given these factors, the present study uses the CLM method for fitting fragility curves as follows:

$$P(DL \geq dl | HIM) = \Phi\left(\hat{\beta}_j + \hat{\beta}_2 ln(HIM)\right) \quad (1)$$

where Φ is the standard cumulative normal distribution function, and the probability (P) to equal or exceed a given damage state is expressed in terms of the hazard intensity metric (HIM). Fragility curves representing damage levels may converge, but will not cross. This is because each cumulative probability has its own intercept ($\hat{\beta}_j$) but shares a common slope coefficient ($\hat{\beta}_2$) satisfying an assumption that higher hazard intensities are required for a higher damage level (Lallemant et al., 2015; Macabuag et al., 2016). When data are treated as nominal rather than ordinal, as is the case for GLMs and OLS data binning, fragility curves are able to cross each other. This can occur when few damage level samples are represented in an empirical dataset. In cases where few observations represent the highest damage level, CLMs will utilise observations for the second highest damage level to fit a representative fragility curve (Lallemant et al., 2015; Williams et al., 2019a).

4. Results

Here we present the RFM results of feature importance and SRC tests for damage sample variables (Section 4.1) and tsunami fragility curves (Section 4.2) for roads (Section 4.2.1) and utility poles (Section 4.2.2).

4.1 Feature importance and correlation tests for damage sample variables

Road and utility pole damage sample variables were applied in RFM and SRC. The RFM identifies the relative importance of tsunami hazard and network component attribute variables in determining physical damage, then SRC confirms importance with correlation of the monotonic relationship. Here, we focus on reporting the importance and relationships of tsunami hazards (hydrodynamic and non-hydrodynamic) and network component attributes for road and utility pole damage.

The RFM indicates scour and debris impact are of high importance for roads and utility pole damage (Figure 3a, c). The SRC tests confirm importance, demonstrating significant positive correlations between damage and scour (0.67-0.68, *p* value <0.01) for roads, and debris impact (0.76, *p* value <0.01) for utility poles (Figure 4a, c). Scour also demonstrates a moderate positive relationship with both interpolated (0.29, *p* value <0.01) and simulated (0.38, *p* value <0.01) flow depth (Figure 4a, b). Simulated flow depth shows a moderate to significant positive relationship with flow velocity and hydrodynamic force, coinciding with a positive monotonic relationship with scour (Figure 4b). This indicates scour is most likely to cause road damage in response to flow velocity and hydrodynamic force increasing with flow depth.

Flow velocity is the simulated hydrodynamic HIM of highest importance for utility pole damage (Figure 4d). A positive monotonic relationship is observed with debris impact, which demonstrates a high importance for causing utility pole damage. Incidence of debris impact for utility poles in built-up areas will be relatively higher when debris entrained in tsunami flows increase in response to increasing flow velocity and hydrodynamic force. Here, Figure 4d demonstrates a positive relationship with all interpolated and simulated hydrodynamic HIMs, indicating debris impact and utility pole damage is more likely as hazard intensity increases. Similarly, scour is a variable of relatively higher importance for utility pole damage (Figure 4c, d), and demonstrates a positive relationship with hydrodynamic HIMs. These observations highlight non-hydrodynamic hazards in response to hydrodynamic HIMs have a key influence on utility pole damage.

Overall, the RFM shows road and utility pole network component attributes have lower importance for physical damage compared to hydrodynamic and non-hydrodynamic hazards. Gini coefficients of <0.05 are observed for most attributes. The exception is for road network components, where distance from coastline and number of lanes exceeded 0.1 relative to the interpolated and simulation hydrodynamic HIMs respectively (Figure 3a, b). Despite a low Gini coefficient, distance from coastline also shows

relatively higher importance for utility pole damage. This is expected as the negative monotonic relationships observed between distance from coastline and hydrodynamic HIMs indicates hazard intensities decrease with distance inland. Lower hazard intensities further reduce the potential for road and utility pole damage from scour or debris impact. While not clearly demonstrated by the RFM, SRC tests demonstrate positive monotonic relationships between damage levels and road (e.g. surface: asphalt and unsealed, capacity: local, culvert) and utility pole (i.e. steel, height < 5m) network component attributes. This highlights the need to consider such attributes in the development of object-specific tsunami fragility curves for roads and utility poles.

4.2 Fragility curves

Tsunami fragility curves are presented here for roads (Section 4.2.1) and utility poles (Section 4.2.2). Fragility curve parameters are reported in Tables 4 and 5. The tsunami fragility curves each reflect a variation in damage probability due to (1) HIM (interpolated depth (m), simulated flow depth (m), flow velocity (m/s) and hydrodynamic force (kN/m), (2) mixed attributes (damage level only), (3) construction material, and (4) capacity (roads).

4.2.1. Roads

A flow depth of 2 m is used here to compare network component vulnerability across curves since this depth has been previously defined as a critical threshold for damage level 3 in particular (Williams, et al., 2019b). The probability of mixed attribute roads (i.e. all construction material and capacity types) reaching or exceeding DL1, DL2 and DL3 at 2 m flow depth is 0.16, 0.09 and 0.07, respectively (Fig. 5a), for interpolated flow depth, and 0.2, 0.11 and 0.08, respectively (Fig. 5b), for simulated flow depth. The results indicate there is a 0.5 probability of reaching or exceeding DL1, DL2 and DL3 at 6.8 m, 10.2 m and 12.4 m flow depth (interpolated) respectively and 5.4 m, 8.4 m, and 10.6 m respectively for flow depth (simulated) for mixed attribute roads (Fig. 5a and b). While a specific value for flow depth (2m) is defined as a critical threshold in literature, this is not the case for flow velocity and hydrodynamic force. Therefore, arbitrary values of 5 m/s and 10 kN/m are used as reference points to compare network component vulnerability across the flow velocity and hydrodynamic force (respectively) fragility curves. The probability of mixed attribute roads reaching or exceeding DL1, DL2 and DL3 at 5 m/s flow velocity is 0.63, 0.46 and 0.38 respectively (Fig. 6a). There is a 0.5 probability of reaching or exceeding DL1, DL2 and DL3 at 4.2 m/s, 5.3 m/s and 5.9 m/s velocity respectively for mixed attribute roads (Fig. 6a). Finally, for hydrodynamic force, a probability of mixed attribute roads reaching or exceeding DL1, DL2 and DL3 at 10 kN/m hydrodynamic force is 0.48, 0.32 and 0.25 respectively (Fig. 6b). There is a 0.5 probability of reaching or exceeding DL1, DL2 and DL3 at 10.6 kN/m, 18.6 kN/m and 25 kN/m hydrodynamic force respectively for mixed attribute roads (Fig. 6b).

There is some difference in DL1 and DL2 exceedance probability for asphalt and concrete road construction materials as tsunami flow increases (Fig. 5c-f), with higher probabilities indicated for

concrete construction over asphalt construction. However there are considerably lower probabilities of DL3 exceedance for concrete construction (e.g. 0.04 at 2 m interpolated flow depth, 0.0 at 2 m simulated flow depth, 0.01 at 5 m/s flow speed and 0.01 at 10 kN/m hydrodynamic force), when compared to asphalt roads (e.g. 0.09, 0.1, 0.55 and 0.35 respectively).

Road capacity, in this study, is used as a proxy for construction standards where field data is absent. Higher capacity ‘collector’ roads are often built to a higher standard than lower capacity ‘local’ roads, and are potentially more resistant to tsunami forces (Williams et al., 2020a, b). In Coquimbo, tsunami fragility curves representing DL1 and DL2 are mostly lower for both collector and local roads (considerably so with flow speed and hydrodynamic force as HIMs). However, collector roads have far lower probability of reaching or exceeding DL3 (e.g. 0.02 at 2 m interpolated flow depth, 0.03 at 2 m simulated flow depth, 0.09 at 5 m/s flow speed and 0.07 at 10 kN/m hydrodynamic force), when compared to local roads (e.g. 0.14, 0.16, 0.84 and 0.54 respectively).

Table 4
Summary of tsunami fragility function parameters for roads. Pseudo r^2 is calculated using the McFadden method (McFadden, 1974)

Fragility function		*μ*	*σ*	*r^2*
Mixed roads DMAX	DL1	1.69	1.20	0.05
	DL2	2.14	1.20	
	DL3	2.36	1.20	
Concrete roads DMAX	DL1	1.38	0.60	0.12
	DL2	1.81	0.60	
	DL3	2.71	0.60	
Asphalt roads DMAX	DL1	1.28	0.86	0.001
	DL2	1.50	0.86	
	DL3	1.60	0.86	
Local roads DMAX	DL1	1.19	0.90	0.08
	DL2	1.57	0.90	
	DL3	1.59	0.90	
Collector roads DMAX	DL1	1.66	0.89	0.08
	DL2	1.98	0.89	
	DL3	2.41	0.89	
Mixed roads VMAX	DL1	1.43	0.56	0.13
	DL2	1.67	0.56	
	DL3	1.78	0.56	
Concrete roads VMAX	DL1	1.58	0.59	0.14
	DL2	2.01	0.59	
	DL3	2.90	0.59	
Asphalt roads VMAX	DL1	1.35	0.47	0.12
	DL2	1.49	0.47	
	DL3	1.55	0.47	
Local roads VMAX	DL1	1.07	0.31	0.34

Fragility function		*μ*	*σ*	r^2
	DL2	1.28	0.31	
	DL3	1.30	0.31	
Collector roads VMAX	DL1	2.30	1.21	0.03
	DL2	2.71	1.21	
	DL3	3.24	1.21	
Mixed roads FMAX	DL1	2.37	1.38	0.13
	DL2	2.94	1.38	
	DL3	3.22	1.38	
Concrete roads FMAX	DL1	2.60	1.31	0.14
	DL2	3.56	1.31	
	DL3	5.52	1.31	
Asphalt roads FMAX	DL1	2.27	1.34	0.02
	DL2	2.65	1.34	
	DL3	2.81	1.34	
Local roads FMAX	DL1	1.61	0.97	0.25
	DL2	2.16	0.97	
	DL3	2.20	0.97	
Collector roads FMAX	DL1	3.99	2.51	0.05
	DL2	4.85	2.51	
	DL3	5.99	2.51	
Mixed roads IDMAX	DL1	1.91	1.22	0.09
	DL2	2.33	1.22	
	DL3	2.53	1.22	
Concrete roads IDMAX	DL1	2.12	1.34	0.12
	DL2	3.04	1.34	
	DL3	4.98	1.34	
Asphalt roads IDMAX	DL1	1.72	0.97	0.05
	DL2	1.92	0.97	

Fragility function		*μ*	*σ*	r^2
	DL3	2.01	0.97	
Local roads IDMAX	DL1	1.44	1.15	0.12
	DL2	1.89	1.15	
	DL3	1.92	1.15	
Collector roads IDMAX	DL1	1.77	0.81	0.10
	DL2	2.03	0.81	
	DL3	2.34	0.81	

4.2.2. Utility poles

The probability of mixed attribute utility poles (i.e. all construction materials and pole heights) reaching or exceeding DL1, DL2 and DL3 at 2 m flow depth is 0.28, 0.17 and 0.13 respectively (Fig. 7a) for interpolated depth and 0.27, 0.20 and 0.19 respectively for simulated depth (Fig. 7b). There is a 0.5 probability of reaching or exceeding DL1, DL2 and DL3 at 3.1 m, 3.9 m and 4.5 m flow depth (interpolated), respectively, (Fig. 7a) and at 4.1 m 5.3 m and 5.6 m flow depth (simulated), respectively (Fig. 7b). The probability of mixed attribute utility poles reaching or exceeding DL1, DL2 and DL3 at 5 m/s flow speed is 0.52, 0.43 and 0.41, respectively (Fig. 8a). There is a 0.5 probability of reaching or exceeding DL1, DL2 and DL3 at 4.8 m/s, 6.1 m/s and 6.4 m/s flow speed, respectively, for mixed attribute utility poles (Fig. 8a). Finally, for flow hydrodynamic force 10 kN/m is used to compare component vulnerability. The probability of mixed attribute utility poles reaching or exceeding DL1, DL2 and DL3 at 10 kN/m hydrodynamic force is 0.49, 0.40 and 0.38 respectively (Fig. 8b). There is a 0.5 probability of reaching or exceeding DL1, DL2 and DL3 at 10.2 kN/m, 16.2 kN/m and 18 kN/m hydrodynamic force respectively for mixed attribute roads (Fig. 8b).

Utility pole construction material appears to influence fragility (Fig. 7c-h). At 2 m flow depth, there is a probability of reaching or exceeding DL1, DL2 and DL3 of 0.08, 0.05 and 0.03 (interpolated) and 0.06, 0.03 and 0.03 (simulated) for concrete poles, 0.40, 0.23 and 0.19 (interpolated) and 0.44, 0.34 and 0.32 (simulated) for steel poles, and 0.36, 0.20 and 0.16 (interpolated) and 0.40, 0.23 and 0.19 (simulated) for timber poles (Fig. 7c-h). The probability of utility poles reaching or exceeding DL1, DL2 and DL3 at 5 m/s flow velocity is 0.21, 0.48 and 0.46 for concrete, steel and timber construction respectively (Fig. 8c, e, g). The probability of utility poles reaching or exceeding DL1, DL2 and DL3 at 10 kN/m hydrodynamic force is 0.07, 0.59 and 0.31, for concrete, steel and timber construction respectively (Fig. 8d, f, h).

Table 5
Summary of tsunami fragility function parameters for utility poles. Pseudo r^2 is calculated using the McFadden method (McFadden, 1974)

Fragility function		*μ*	*σ*	*r²*
Mixed poles DMAX	DL1	1.41	1.15	0.05
	DL2	1.67	1.15	
	DL3	1.72	1.15	
Concrete poles DMAX	DL1	5.50	3.04	0.02
	DL2	6.29	3.04	
	DL3	6.47	3.04	
Steel poles DMAX	DL1	0.79	0.67	0.08
	DL2	0.97	0.67	
	DL3	1.01	0.67	
Timber poles DMAX	DL1	4.32	13.43	0.00
	DL2	11.70	14.98	
	DL3	13.61	15.26	
Mixed poles VMAX	DL1	1.56	1.12	0.04
	DL2	1.81	1.12	
	DL3	1.87	1.12	
Concrete poles VMAX	DL1	1.91	0.66	0.10
	DL2	2.10	0.66	
	DL3	2.14	0.66	
Steel poles VMAX	DL1	1.15	1.87	0.01
	DL2	1.62	1.87	
	DL3	1.72	1.87	
Timber poles VMAX	DL1	1.07	1.03	0.04
	DL2	1.59	1.03	
	DL3	1.70	1.03	
Mixed poles FMAX	DL1	2.33	2.06	0.07

Fragility function		*μ*	*σ*	r^2
	DL2	2.81	2.06	
	DL3	2.91	2.06	
Concrete poles FMAX	DL1	5.30	2.70	0.06
	DL2	6.03	2.70	
	DL3	6.19	2.70	
Steel poles FMAX	DL1	1.31	1.78	0.06
	DL2	1.78	1.78	
	DL3	1.88	1.78	
Timber poles FMAX	DL1	1.86	4.12	0.02
	DL2	3.92	4.12	
	DL3	4.39	4.12	
Mixed poles IDMAX	DL1	1.11	0.73	0.19
	DL2	1.40	0.73	
	DL3	1.50	0.73	
Concrete poles IDMAX	DL1	2.43	1.23	0.13
	DL2	2.71	1.23	
	DL3	2.99	1.23	
Steel poles IDMAX	DL1	0.86	0.69	0.17
	DL2	1.20	0.69	
	DL3	1.30	0.69	
Timber poles IDMAX	DL1	1.05	0.98	0.08
	DL2	1.53	0.98	
	DL3	1.65	0.98	

5. Discussion

Flow depth is the key HIM for many tsunami fragility curves (Section 1; Koshimura et al., 2009; Suppasri et al., 2013), however, other hydrodynamic HIMs are often cited as being more important (De Risi et al., 2017; J Macabuag et al., 2016; Song et al., 2017). Here we analysed the relative importance of flow depth

(interpolated and simulated), flow velocity and hydrodynamic force. Flow depth showed high importance for physical damage to roads and utility poles (Section 4.1). This is not to say that hydrodynamic features of tsunamis are un-important with respect to direct damage impacts, and it is likely these factors contribute to direct damage through other actions. Non-hydrodynamic hazards, such as scour and debris impact, showed high importance for physical damage and were likely have exacerbated damage.

Scour, being the strongest variable in RFM and SRC testing (Figure 3 and Figure 4) for roads (and second highest for utility poles), and debris impact the strongest for utility poles, demonstrates a clear need to further investigate the non-hydrodynamic impacts from tsunamis. The next steps would be to determine when and where scour and debris impact is most important with further investigation into the relationships between hydrodynamic force, soil conditions (scour) and land-use that could lead to scour and debris potential. Previous studies have investigated debris potential for tsunami impact assessment of buildings (J Macabuag et al., 2016; Naito et al., 2014; Shafiei et al., 2016). However, the only example of debris-based fragility assessment for roads is Williams et al. (2020a), which investigates the relationship between debris deposition and road service rather than debris impact and damage level.

This work, for scour and debris impact, could be undertaken with existing tsunami impact datasets (e.g. Tohoku 2011, Illapel 2015, and Sulawesi 2018) and progressed further by subsequent field observations. Ultimately this could progress the tsunami hazard field, beyond the use of traditional hazard maps for impact assessment, by enhancing these with non-hazard parameters (debris potential, land-use, ground conditions etc.). The importance of scour for component damage presented in this study is supported by previous studies (J. Chen et al., 2013; Yeh et al., 2013) that have observed considerable scour-based damage for roads. Notably, the distribution of scour observed in the 2018 Sulawesi tsunami (Paulik et al., 2019; Williams et al., 2020b), in that high concentrations were observed along a coastal esplanade and low concentrations observed >50 m from the shoreline is consistent with that observed in the Illapel event (i.e. along Avineda Costanera), which are comparable in relative size. This may indicate a relative importance of the scour-causing conditions (e.g. ground conditions and land-use) for relatively small tsunami events in contrast to larger subduction zone events (e.g. IOT and Tohoku) where scour is still observed at high concentrations further inland (i.e. >50m).

There is a positive monotonic relationship between flow depth and both flow velocity and hydrodynamic force in the SRC tests (Figure 3). This indicates flow depth could be a fair proxy for flow velocity and hydrodynamic force, and vice versa, in the application of fragility curves. This is consistent with previous studies (Maruyama and Itagaki, 2017; Williams, et al. 2020b; Williams, et al. 2020a) that propose, but do not test, this relationship. However, this is inconsistent with a number of studies (Song et al., 2017; Wang et al., 2020) that claim flow depth is not a reliable metric for assessing tsunami hazard and damage relationships. One implication of this finding is that while velocity and hydrodynamic force are important HIMs, flow depth is of the greatest importance, and could therefore be used as a reliable proxy for tsunami exposure, impact and risk assessment. More work should be done in the future to correlate these network component and HIM relationships. As interpolated flow depth is the most commonly used HIM for fragility assessment (e.g. Koshimura et al., 2009; Maruyama and Itagaki, 2017; Mas et al., 2020). This,

and future, suites of empirical and numerical tsunami fragility curves could be applied to refine tsunami impact and risk assessment with the likes of HIM weightings supported by variable correlation testing (i.e. from this study and future studies).

Roads in Coquimbo performed poorly when compared with the 2011 Tohoku event, and performed considerably well when compared with the 2018 Sulawesi event (Figure 9). In the 2011 Tohoku tsunami, the probability of complete damage (i.e. DL3) at 5 m flow depth was 0.10 (Williams et al., 2020a), compared to 0.23 (interpolated depth) and 0.27 (simulated depth) reported in the present study (Figure 9a). It should be noted that these use a GLM method, with manual data binning, as do the Illapel fragility curves from the same study. Using the same dataset, but different fragility function development methods (Section 3.4), Coquimbo roads are shown to perform worse in the present study (e.g. 0.53 probability of exceeding/reaching DL3 at 5m (interpolated depth) and 0.27 (simulated depth)) than indicated by Williams et al. (2020), (e.g. 0.12 probability of reaching or exceeding DL3 at 5m). The CLM method, used in the present study, is considered to be appropriate for fitting curves to datasets of this nature (Lallemant et al., 2015; Williams et al., 2019a; Williams et al., 2020b), implying that this study has refined the event fragility curves in a way that would have considerably higher levels of damage modelled for subsequent impact and risk assessments. This study, therefore, represents a considerable improvement to the field, and a case could be made to similarly improve the comparable road component fragility curves for the 2011 Tohoku tsunami event (Graf et al., 2014; Williams et al., 2020a). The most directly comparable previous study for road fragility curves are from the 2018 Sulawesi tsunami (also CLM method), which has a 0.57 probability of reaching or exceeding DL3 at 5 m flow depth (Williams et al., 2020b). With respect to utility poles, the low threshold for pole damage (e.g. 0.56 of reaching or exceeding DL3 at 5m (interpolated depth) and 0.46 (simulated depth) is lower in the present study, compared to pole fragility analysed for the 2018 Sulawesi tsunami (e.g. 0.86 of reaching or exceeding DL3 at 5m).

It is crucial that the local hazard and network component conditions are considered when applying tsunami fragility curves. The 2015 Illapel tsunami was a relatively small tsunami by historical standards. It was also documented as producing relatively long wave-lengths given its regional subduction zone earthquake origins – meaning a slow deterioration of wave energy inland (Heidarzadeh et al., 2015). Comparably, with the only other available suite of CLM tsunami fragility curves for infrastructure network components for an event of this magnitude, the 2018 Sulawesi tsunami was documented as a notably short wave-length (traveling ~0.3 km inland), given its locally sourced earthquake and landslide induced origins (Aránguiz et al., 2020). Conversely, the 2011 Tohoku tsunami, which has GLM fragility curves for infrastructure network components available (Williams et al., 2020a), was documented as having considerable long wave-lengths (traveling ~11 km inland). The fragility curves developed in this study would not be appropriate to apply for events of higher or smaller wavelengths, as much as the other events' (Sulawesi and Tohoku) fragility curves would not necessarily be appropriate for an event comparable to the 2015 Illapel tsunami. On a similar note, the levels of shaking experienced in each respective case-study, and therefore it's bearing on interpolated component damage levels, varies considerably (11.5 – 21.5 g in Miyagi and Iwate Prefectures (Tohoku) and 11.5 – 40.1 g in Palu

(Sulawesi) and compared with 0.20–0.29 g in Coquimbo (Illapel)) and should be considered in any application of fragility curves for impact and risk assessment (USGS, 2015). The growing catalogue of post-event empirical component damage, hazard and fragility datasets, provides wider scope for increasingly sophisticated and credible tsunami impact assessment, of which will ultimately inform tsunami risk reduction globally.

6. Conclusions

This study analyses tsunami vulnerability infrastructure network components damaged in the 2015 Illapel tsunami at Coquimbo, Chile. Hydrodynamic HIMs from interpolated and simulated tsunami hazard models for the event were used to develop fragility curves for roads and utility poles. A four-level classification of structural damage was used, from 'No damage' through to 'Complete damage'. The methodology applied in this paper overcomes the limitations of in-field tsunami hazard surveys by incorporating simulated hydrodynamic models, the HIMs of which were not possible to capture from field surveys alone.

A Random Forest Model and Spearman's Rank correlation test were applied to analyse variable importance and monotonic relationships between tsunami hazards and critical infrastructure network component damage levels (DL). These models and tests revealed scour for roads and debris impact and scour for utility poles, are highly important and strongly correlated with damage levels. Of the hazard specific variables flow depth is the strongest and has the highest correlation with damage levels flow while flow velocity and hydrodynamic force are also important but considerably second and third to depth. The SRC tests also demonstrate that flow depth is strongly correlated with flow velocity and hydrodynamic force, indicating it could be a fair proxy for velocity and force, and vice versa.

This hybrid hazard methodology provided a higher-resolution of the resultant fragility curves than previous studies. The cumulative link model methodology used to develop fragility curves represents a considerable improvement to the previously developed general link model fragility curves for the same road damage dataset. Roads demonstrate both higher and lower vulnerability compared to those analysed in previous events, with 0.23 probability of reaching or exceeding DL3 at 5 m flow depth, compared with 0.1 and 0.57 for the 2011 Tohoku tsunami and 2018 Sulawesi tsunami, respectively. Utility poles demonstrate lower vulnerability than those exposed in the 2018 Sulawesi tsunami, with a 0.56 and 0.86 probability of reaching or exceeding DL3 respectively. These curves can be applied to future assessments of impact due to potential tsunamis. Application of the synthesised fragility curves in other areas should be carefully evaluated considering the uncertainties of local hazard and network component characteristics.

Declarations

Funding:

This study was funded by the National Institute of Water and Atmospheric Research (NIWA) Taihoro Nukurangi Strategic Scientific Interest Fund work programme on “Hazard Exposure and Vulnerability” [CARH2206].

Competing Interests:

The authors have no competing interests to declare.

Data availability:

The data that support the findings of this study are available from the corresponding author upon reasonable request.

References

1. Aránguiz, R., Esteban, M., Takagi, H., Mikami, T., Takabatake, T., Gómez, M., … Nistor, I. (2020). The 2018 Sulawesi tsunami in Palu city as a result of several landslides and coseismic tsunamis. *Coastal Engineering Journal*, *62*(4), 445–459. https://doi.org/10.1080/21664250.2020.1780719
2. Aránguiz, R., González, G., González, J., Catalán, P. A., Cienfuegos, R., Yagi, Y., … Rojas, C. (2016). The 16 September 2015 Chile Tsunami from the Post-Tsunami Survey and Numerical Modeling Perspectives. *Pure and Applied Geophysics*, *173*(2), 333–348. https://doi.org/10.1007/s00024-015-1225-4
3. Aránguiz, R., Urra, L., Okuwaki, R., Yagi, Y. (2018). Development and application of a tsunami fragility curve of the 2015 tsunami in Coquimbo, Chile. *Natural Hazards and Earth System Sciences*, *18*(8), 2143–2160. https://doi.org/10.5194/nhess-18-2143-2018
4. Ballantyne, D. (2006). Sri Lanka lifelines after the December 2004 Great Sumatra earthquake and tsunami. *Earthquake Spectra*, *22*(SUPPL. 3), 545–559. https://doi.org/10.1193/1.2211367
5. Bojorquez, E., Iervolino, I., Reyes-Salazar, A., Ruiz, S. E. (2012). Comparing vector-valued intensity measures for fragility analysis of steel frames in the case of narrow-band ground motions. *Engineering Structures*, *45*, 472–480. https://doi.org/10.1016/j.engstruct.2012.07.002
6. Breiman, L. (2001). Random forests. *Machine Learning*, *45*, 5–32. https://doi.org/https://doi.org/10.1023/A:1010933404324
7. Charvet, I., Ioannou, I., Rossetto, T., Suppasri, A., Imamura, F. (2014). Empirical fragility assessment of buildings affected by the 2011 Great East Japan tsunami using improved statistical models. *Natural Hazards*, *73*(2), 951–973. https://doi.org/10.1007/s11069-014-1118-3
8. Chen, C, Melville, B. W. (2015). EXPERIMENTAL STUDY OF UPLIFT PRESSURES ON WHARF DECKS DUE TO TSUNAMI BORES. In *36th IAHR World Congress, 28 June - 3 July, 2015*. The Hague, The

Netherlands: E-proceedings of the 36th IAHR World Congress, 2015. Retrieved from https://researchspace.auckland.ac.nz/handle/2292/27900

9. Chen, Cheng, Melville, B. W., Nandasena, N. A. K., Farvizi, F. (2018). An Experimental Investigation of Tsunami Bore Impacts on a Coastal Bridge Model with Different Contraction Ratios. *Journal of Coastal Research*, *342*, 460–469. https://doi.org/10.2112/jcoastres-d-16-00128.1
10. Chen, Cheng, Melville, B. W., Nandasena, N. A. K., Shamseldin, A. Y., Wotherspoon, L. (2017). Mitigation Effect of Vertical Walls on a Wharf Model Subjected to Tsunami Bores. *Journal of Earthquake and Tsunami*, *11*(3), 1–19. https://doi.org/10.1142/S179343111750004X
11. Chen, J., Huang, Z., Jiang, C., Deng, B. (2013). Tsunami-induced scour at coastal roadways : a laboratory study. *Natural Hazards*, *69*, 655–674. https://doi.org/10.1007/s11069-013-0727-6
12. Chua, C. T., Switzer, A. D., Suppasri, A., Li, L., Pakoksung, K., Lallemant, D., … Cheong, A. (2020). Tsunami damage to ports : Cataloguing damage to create fragility functions from the 2011 Tohoku event. *NHESS*, *in review*, 1–37. Retrieved from https://doi.org/10.5194/nhess-2020-355
13. Contreras-López, M., Winckler, P., Sepúlveda, I., Andaur-Álvarez, A., Cortés-Molina, F., Guerrero, C. J., … Figueroa-Sterquel, R. (2016). Field Survey of the 2015 Chile Tsunami with Emphasis on Coastal Wetland and Conservation Areas. *Pure and Applied Geophysics*, *173*, 349–367. https://doi.org/10.1007/s00024-015-1235-2
14. De Risi, R., Goda, K., Yasuda, T., Mori, N. (2017). Is flow velocity important in tsunami empirical fragility modeling? *Earth-Science Reviews*, *166*, 64–82. https://doi.org/10.1016/j.earscirev.2016.12.015
15. Edwards, C. (2006). Thailand lifelines after the December 2004 Great Sumatra earthquake and Indian Ocean tsunami. *Earthquake Spectra*, *22*(SUPPL. 3), S641–S659. https://doi.org/10.1193/1.2204931
16. Eguchi, R. T., Eguchi, M. T., Bouabid, J., Koshimura, S., Graf, W. P. (2013). *HAZUS Tsunami Benchmarking, Validation and Calibration*. *Prepared for the Federal Emergency Management Agency through a contract with Atkins*. Retrieved from https://nws.weather.gov/nthmp/2013mesmms/abstracts/TsunamiHAZUSreport.pdf
17. ESRI contributors. (2020). 'Topographic' [basemap]. Scale Not Given. https://www.arcgis.com/home/item.html?id=30e5fe3149c34df1ba922e6f5bbf808f. Accessed 20 March 2020,
18. Evans, N. L., McGhie, C. (2011). The Performance of Lifeline Utilities following the 27 th February 2010 Maule Earthquake Chile. In *9th Pacific Conference on Earthquake Engineering, Building an Earthquake-Resilient Society, 14-16 April, 2011*. Auckland, New Zealand. Retrieved from https://www.nzsee.org.nz/db/2011/036.pdf
19. Fritz, H. M., Petroff, C. M., Catalán, P. a., Cienfuegos, R., Winckler, P., Kalligeris, N., … Synolakis, C. E. (2011). Field Survey of the 27 February 2010 Chile Tsunami. *Pure and Applied Geophysics*, *168*(11), 1989–2010. https://doi.org/10.1007/s00024-011-0283-5
20. Gehl, P., D'Ayala, D. (2015). Integrated Multi-Hazard Framework for the Fragility Analysis of Roadway Bridges. In *12th International Conference on Applications ofStatistics and Probability in Civil*

Engineering, ICASP12, 12-15 July, 2015 (pp. 1–8). Vancouver, Canada. Retrieved from https://www.infrarisk-fp7.eu/sites/default/files/docs/Paper_343_Gehl.pdf

21. Goff, J., Liu, P. L. F., Higman, B., Morton, R., Jaffe, B. E., Fernando, H., … Fernandoj, S. (2006). Sri Lanka field survey after the December 2004 Indian Ocean tsunami. *Earthquake Spectra*, *22*(SUPPL. 3), 155–172. https://doi.org/10.1193/1.2205897
22. Graf, W. P., Lee, Y., Eguchi, R. T. (2014). New Lifelines Damage and Loss Functions for Tsunami. In *Tenth U.S. National Conference on Earthquake Engineering Frontiers of Earthquake Engineering, 21-25, July, 2014* (p. 11). Anchorage, USA: Earthquake Engineering Research Institute. Retrieved from https://datacenterhub.org/resources/11732/download/10NCEE-000350.pdf
23. Heidarzadeh, M., Murotani, S., Satake, K., Ishibe, T., Gusman, A. R. (2015). Source model of the 16 September 2015 Illapel, Chile Mw 8.4 earthquake based on teleseismic and tsunami data. *Geophysical Research Letters*, (SEPTEMBER), 643–650. https://doi.org/10.1002/2015GL067297
24. Jamelot, A., Gailler, A., Heinrich, P., Vallage, A., Champenois, J. (2019). Tsunami Simulations of the Sulawesi Mw 7.5 Event: Comparison of Seismic Sources Issued from a Tsunami Warning Context Versus Post-Event Finite Source. *Pure and Applied Geophysics*, *176*(8). https://doi.org/10.1007/s00024-019-02274-5
25. Kawashima, K., Buckle, I. (2013). Structural performance of bridges in the Tohoku-oki earthquake. *Earthquake Spectra*, *29*(SUPPL.1), S315–S338. https://doi.org/10.1193/1.4000129
26. Klapp, J., Areu-Rangel, O. S., Cruchaga, M., Aránguiz, R., Bonasia, R., Godoy, M. J., Silva-Casarín, R. (2020). Tsunami hydrodynamic force on a building using a SPH real-scale numerical simulation. *Natural Hazards*, *100*(1), 89–109. https://doi.org/10.1007/s11069-019-03800-3
27. Koks, E. E., Rozenberg, J., Zorn, C., Tariverdi, M., Vousdoukas, M., Fraser, S. A., … Hallegatte, S. (2019). A global multi-hazard risk analysis of road and railway infrastructure assets. *Nature Communications*, *10*(1), 1–11. https://doi.org/10.1038/s41467-019-10442-3
28. Koshimura, S., Namegaya, Y., Yanagisawa, H. (2009). Tsunami Fragility — A New Measure to Identify Tsunami Damage —. *Journal of Disaster Research*, *4*(6), 479–488. https://doi.org/10.20965/jdr.2009.p0479
29. Lallemant, D., Kiremidjian, A., Burton, H. (2015). Statistical procedures for developing earthquake damage fragility curves. *Earthquake Engineering & Structural Dynamics*, *44*(9), 1373–1389. https://doi.org/10.1002/eqe.2522
30. Li, L., Lay, T., Cheung, K. F., Ye, L. (2016). Joint modeling of teleseismic and tsunami wave observations to constrain the 16 September 2015 Illapel, Chile, Mw 8.3 earthquake rupture process. *Geophysical Research Letters*, *43*(9), 4303–4312. https://doi.org/10.1002/2016GL068674
31. Macabuag, J, Rossetto, T., Ioannou, I. (2016). Investigation of the Effect of Debris-Induced Damage for Constructing Tsunami Fragility Curves for Buildings. In *1st International Conference on Natural Hazards & Infrastructure* (pp. 1–16). Chania, Greece. https://doi.org/10.3390/geosciences8040117
32. Macabuag, Joshua, Rossetto, T., Ioannou, I., Suppasri, A., Sugawara, D., Adriano, B., … Koshimura, S. (2016). A proposed methodology for deriving tsunami fragility functions for buildings using

optimum intensity measures. *Natural Hazards*, *84*(2), 1257–1285. https://doi.org/10.1007/s11069-016-2485-8

33. Maruyama, Y., Itagaki, O. (2017). Development of tsunami fragility functions for ground-level roads. *Journal of Disaster Research*, *12*(1), 131–136. https://doi.org/10.20965/jdr.2017.p0131
34. Mas, E., Paulik, R., Pakoksung, K., Adriano, B., Moya, L., Suppasri, A., … Koshimura, S. (2020). Characteristics of Tsunami Fragility Functions Developed Using Different Sources of Damage Data from the 2018 Sulawesi Earthquake and Tsunami. *Pure and Applied Geophysics*, *177*(6), 2437–2455. https://doi.org/10.1007/s00024-020-02501-4
35. MLIT. (2012). Archive of the Great East Japan Earthquake Tsunami disaster urban reconstruction assistance survey. http://fukkou.csis.u-tokyo.ac.jp/. Accessed 1 June 2015,
36. Naito, C., Cercone, C., S.M.ASCE, Riggs, H. R., S.M.ASCE, Cox, D. (2014). Procedure for Site Assessment of the Potential for Tsunami Debris Impact. *Journal of Waterway, Port, Coastal, and Ocean Engineering*, *140*(2), 223–232. https://doi.org/doi:10.1061/(ASCE)WW.1943-5460.0000222
37. ONEMI. (2015). Monitoreo por Sismo de Mayor Intensidad. https://www.onemi.gov.cl/alerta/se-declara-alerta-roja-por-sismo-de-mayor-intensidad-y-alarma-de-tsunami/. Accessed 26 October 2021,
38. Palliyaguru, R., Amaratunga, D. (2008). Managing disaster risks through quality infrastructure and vice versa. *Structural Survey*, *26*(5), 426–434. https://doi.org/doi:10.1108/02630800810922766
39. Paulik, R., Gusman, A., Williams, J. H., Pratama, G. M., Lin, S., Prawirabhakti, A., … Suwarni, N. W. I. (2019). Tsunami Hazard and Built Environment Damage Observations from Palu City after the September 28 2018 Sulawesi Earthquake and Tsunami. *Pure and Applied Geophysics*, *176*(8), 3305–3321. https://doi.org/10.1007/s00024-019-02254-9
40. Paulik, R., Williams, J. H., Horspool, N., Catalan, P. A., Mowll, R., Cortés, P., Woods, R. (2021). The 16 September 2015 Illapel Earthquake and Tsunami: Post-Event Tsunami Inundation, Building and Infrastructure Damage Survey in Coquimbo, Chile. *Pure and Applied Geophysics*, (September 2015). https://doi.org/10.1007/s00024-021-02734-x
41. Rossetto, T., Ioannou, I., Grant, D., Maqsood, T. (2014). Guidelines for the empirical vulnerability assessment. *GEM Technical Report*, *08*, 140. https://doi.org/10.13117/ GEM.VULN-MOD.TR2014.11
42. Scawthorn, C., Ono, Y., Iemura, H., Ridha, M., Purwanto, B. (2006). Performance of lifelines in Banda Aceh, Indonesia, during the December 2004 Great Sumatra earthquake and tsunami. *Earthquake Spectra*, *22*(SUPPL. 3), 511–544. https://doi.org/10.1193/1.2206807
43. Shafiei, S., Melville, B. W., Shamseldin, A. Y., Beskhyroun, S., Adams, K. N. (2016). Measurements of tsunami-borne debris impact on structures using an embedded accelerometer. *Journal of Hydraulic Research*, *54*(4), 435–449. https://doi.org/10.1080/00221686.2016.1170071
44. Shoji, G., Moriyama, T. (2007). Evaluation of the Structural Fragility of a Bridge Structure Subjected to a Tsunami Wave Load. *Journal of Natural Disaster Science*, *29*(2), 73–81. https://doi.org/10.2328/jnds.29.73
45. Song, J., De Risi, R., Goda, K. (2017). Influence of flow velocity on tsunami loss estimation. *Geosciences (Switzerland)*, *7*(4). https://doi.org/10.3390/geosciences7040114

46. Suppasri, A., Mas, E., Charvet, I., Gunasekera, R., Imai, K., Fukutani, Y., … Imamura, F. (2013). Building damage characteristics based on surveyed data and fragility curves of the 2011 Great East Japan tsunami. *Natural Hazards*, *66*(2), 319–341. https://doi.org/10.1007/s11069-012-0487-8
47. Tang, A., Ames, D., McLaughlin, J., Murugesh, G., Plant, G., Yashinsky, M., … Gandhi, P. (2006). Coastal Indian lifelines after the 2004 Great Sumatra earthquake and Indian Ocean tsunami. *Earthquake Spectra*, *22*(SUPPL. 3), 607–639. https://doi.org/10.1193/1.2206089
48. Tarbotton, C., Dall'Osso, F., Dominey-Howes, D., Goff, J. (2015). The use of empirical vulnerability functions to assess the response of buildings to tsunami impact: Comparative review and summary of best practice. *Earth-Science Reviews*, *142*, 120–134. https://doi.org/10.1016/j.earscirev.2015.01.002
49. Tomita, T., Arikawa, T., Takagawa, T., Honda, K., Chida, Y., Sase, K., Olivares, R. A. O. (2016). Results of Post-Field Survey on the Mw 8.3 Illapel Earthquake Tsunami in 2015. *Coastal Engineering Journal*, *58*(2). https://doi.org/10.1142/S0578563416500030
50. USGS. (2015). U.S. GeologicalSurvey. http://www.usgs.gov/. Accessed 28 October 2021,
51. Wang, X., Power, W., Lukovic, B., Mueller, C., Liu, Y. (2020). A pilot study on effectiveness of flow depth as sole intensity measure of tsunami damage potential. In *NZSEE 2020 Anual Conference*. Retrieved from https://repo.nzsee.org.nz/handle/nzsee/1740
52. Williams, G. T., Kennedy, B. M., Lallemant, D., Wilson, T. M., Allen, N., Scott, A., Jenkins, S. F. (2019). Tephra cushioning of ballistic impacts: Quantifying building vulnerability through pneumatic cannon experiments and multiple fragility curve fitting approaches. *Journal of Volcanology and Geothermal Research*, *388*, 106711. https://doi.org/10.1016/j.jvolgeores.2019.106711
53. Williams, J. H., Paulik, R., Wilson, T. M., Wotherspoon, L., Rusdin, A., Pratama, G. M. (2020). Tsunami Fragility Functions for Road and Utility Pole Assets Using Field Survey and Remotely Sensed Data from the 2018 Sulawesi Tsunami, Palu, Indonesia. *Pure and Applied Geophysics*, 1–28. https://doi.org/10.1007/s00024-020-02545-6
54. Williams, J. H., Wilson, T., Horspool, N., Paulik, R., Wotherspoon, L., Lane, E. M., Hughes, M. W. (2020). Assessing transportation vulnerability to tsunamis: utilising post-event field data from the 2011 Tōhoku tsunami, Japan, and the 2015 Illapel tsunami, Chile. *Natural Hazards and Earth System Sciences*, *20*(2), 451–470. https://doi.org/10.5194/nhess-20-451-2020
55. Yeh, H., Sato, S., Tajima, Y. (2013). The 11 March 2011 East Japan Earthquake and Tsunami: Tsunami Effects on Coastal Infrastructure and Buildings. *Pure and Applied Geophysics*, *170*(6–8), 1019–1031. https://doi.org/10.1007/s00024-012-0489-1

Figures

Figure 1

a) Location of Coquimbo region in South America. b) Coquimbo city. (Basemap source ESRI contributors 2020)

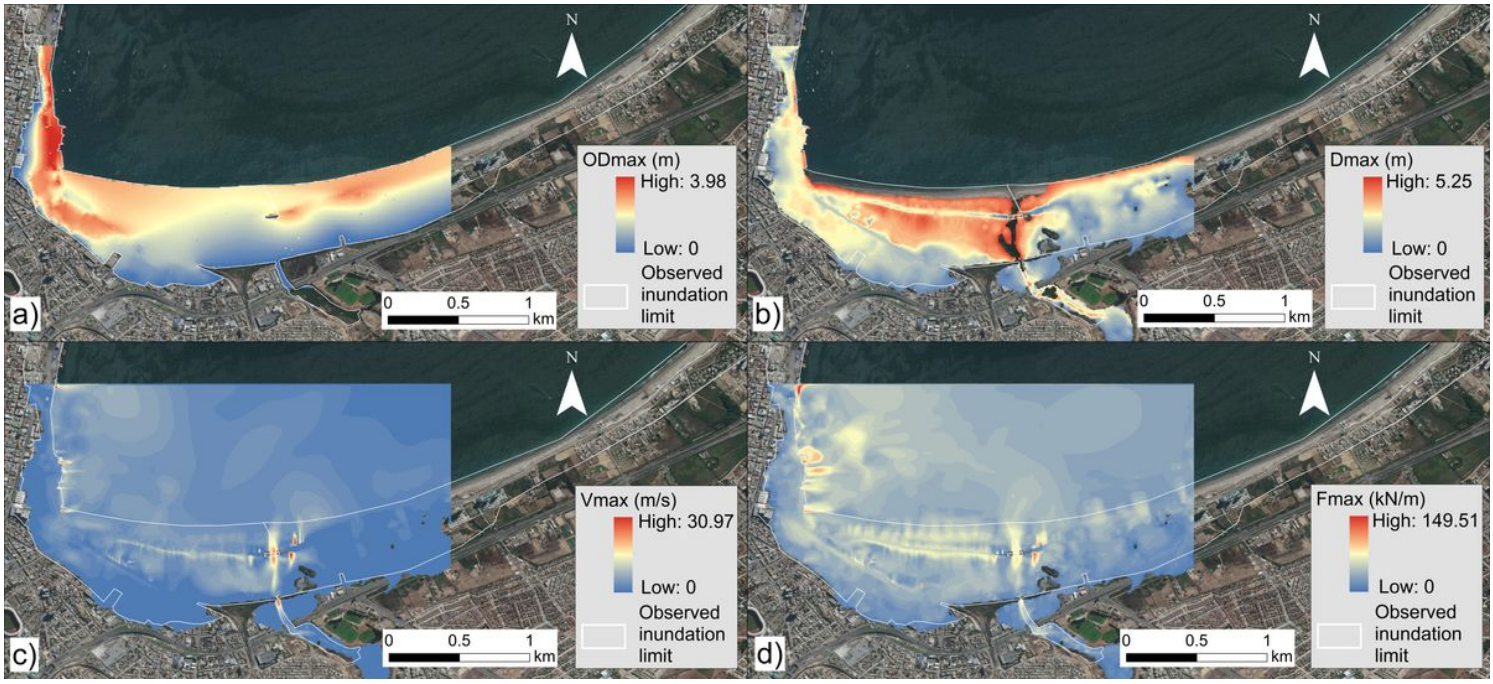

Figure 2

Tsunami interpolation and numerical simulations for (a) interpolated flow depth (b) simulated flow depth, (c) flow velocity and (d) hydrodynamic force hazard intensity measures

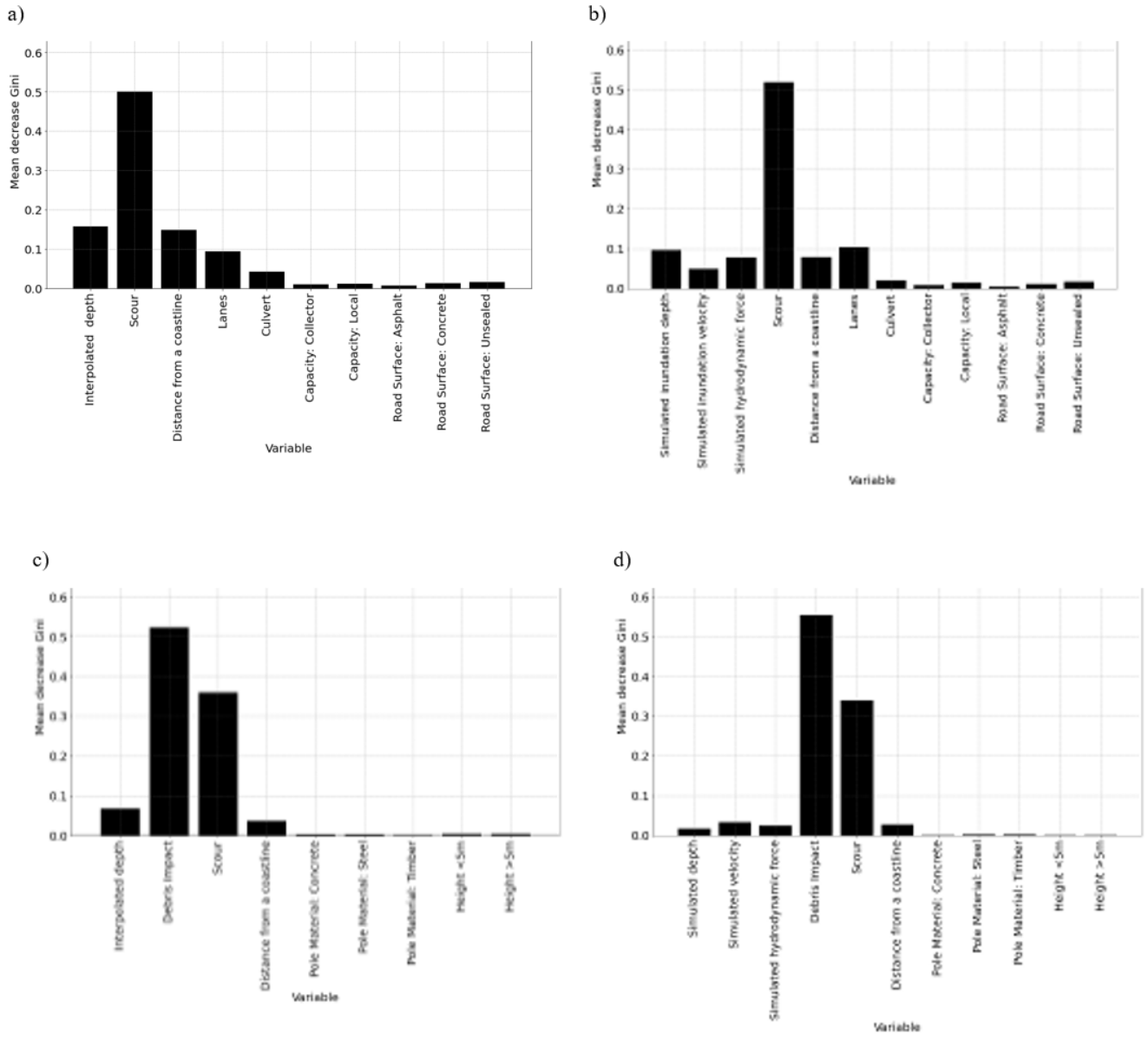

Figure 3

Random forest model feature importance for DRb variables. a) roads interpolated dataset b) roads simulated dataset, c) utility poles interpolated dataset and d) utility poles simulated dataset

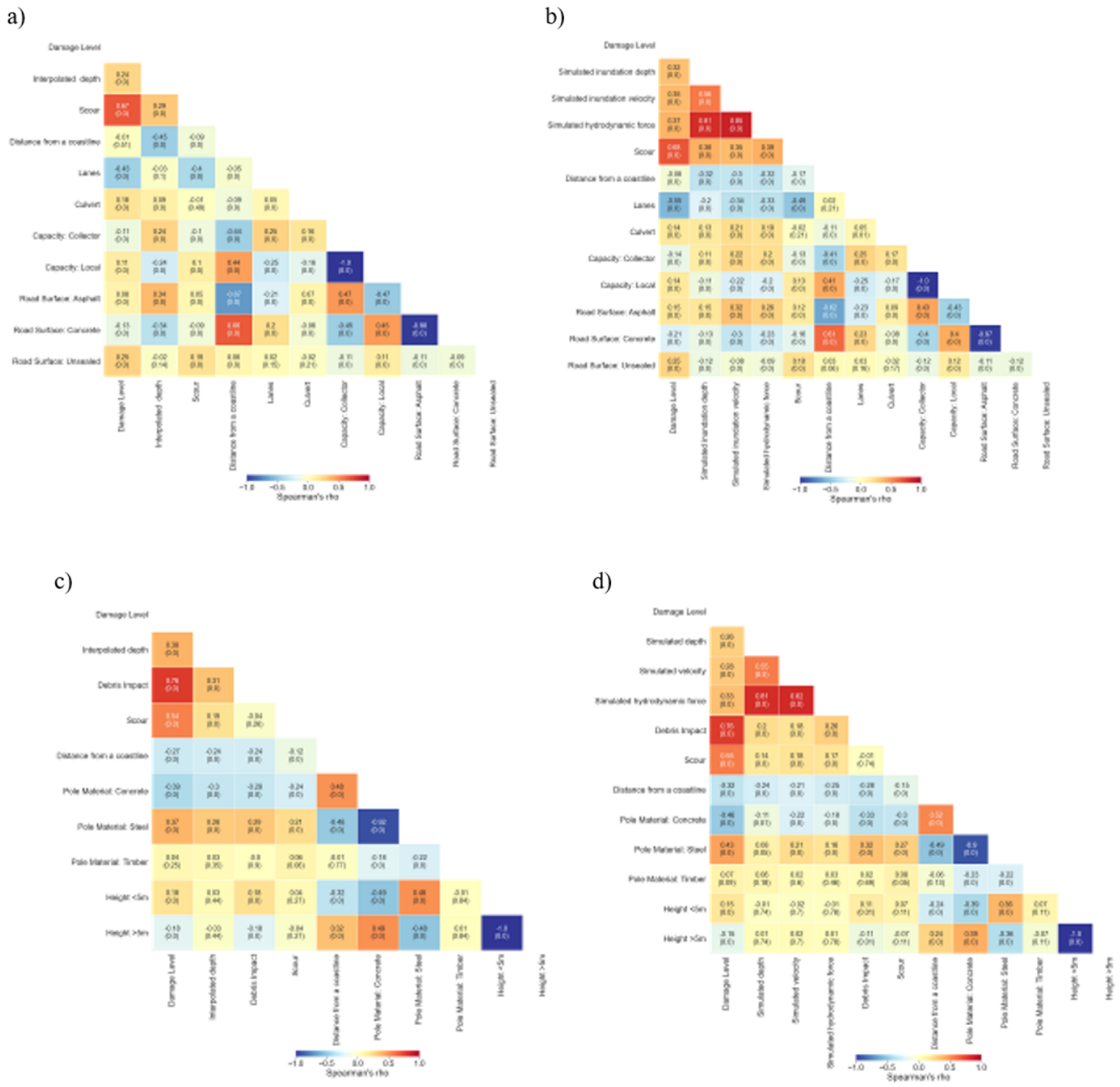

Figure 4

Spearman's rank correlation matrix presenting the rho and significance (p) (below rho) values of tsunami hazard and component attribute variable correlation with DL. a) roads interpolated dataset, b) roads simulated dataset, c) utility poles interpolated dataset and d) utility poles simulated dataset

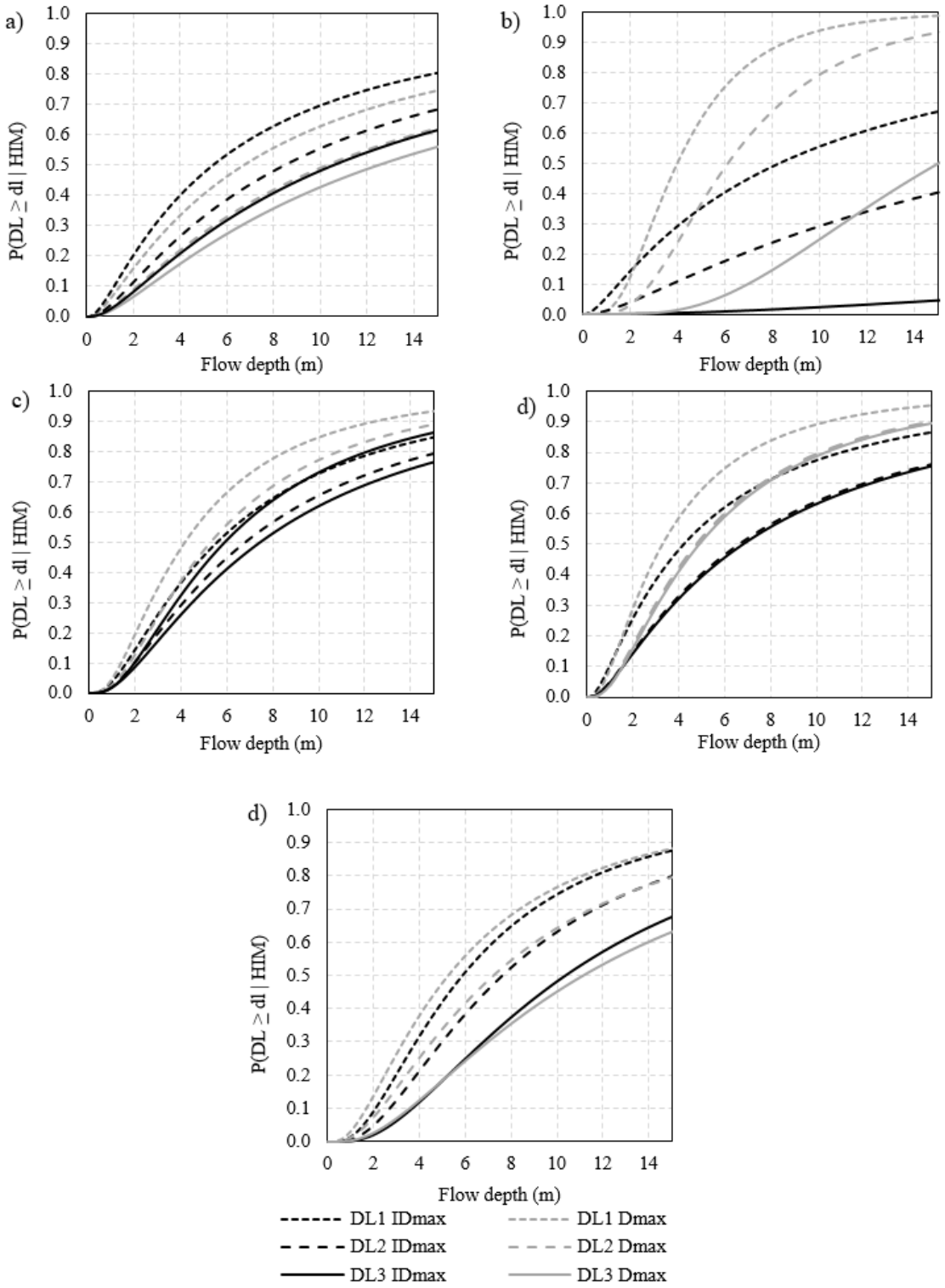

Figure 5

Tsunami fragility curves using IDmax and Dmax for mixed road attributes (a), concrete (b) and asphalt (c) construction roads, and local (d) and collector (e) capacity roads

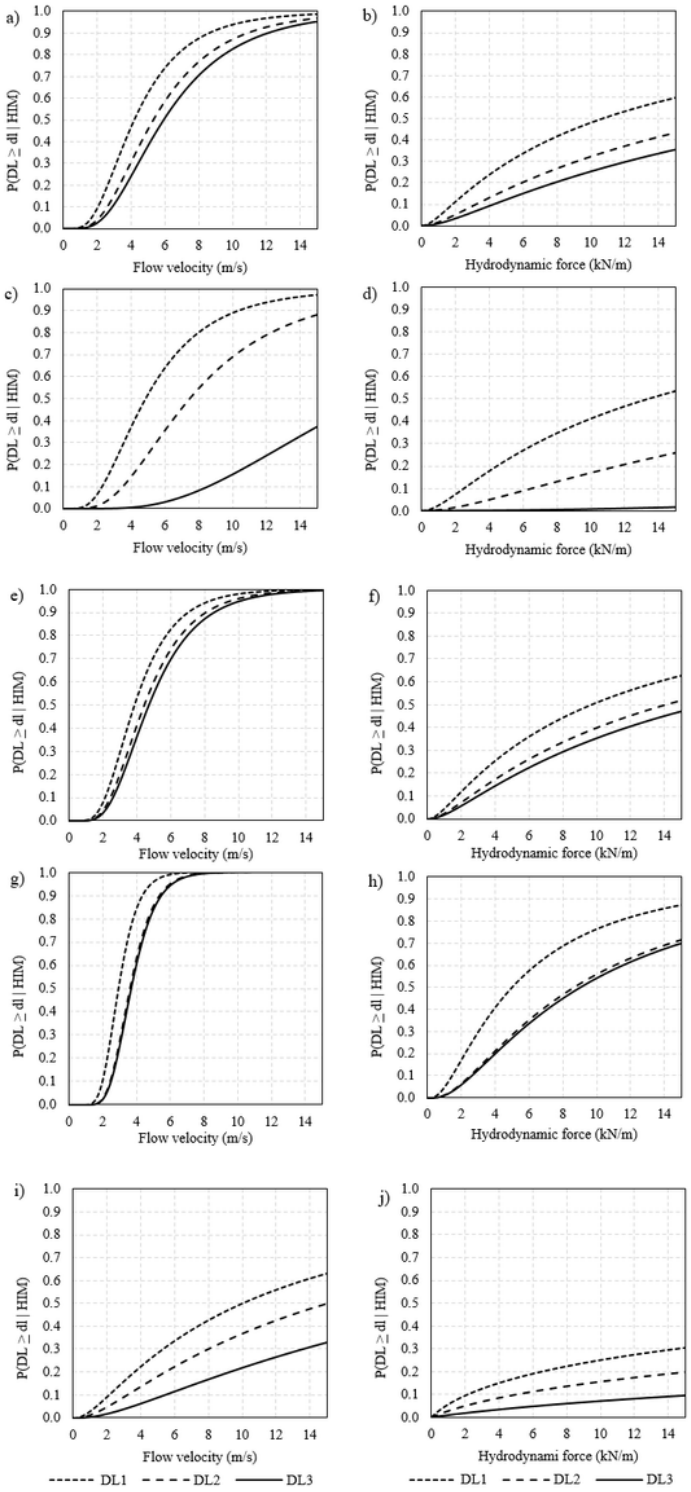

Figure 6

Tsunami fragility curves using Vmax and Fmax (left to right) for mixed road attributes (a, b), concrete (c, d) and asphalt (e, f) construction roads, and local (g, h) and collector (i, j) capacity roads

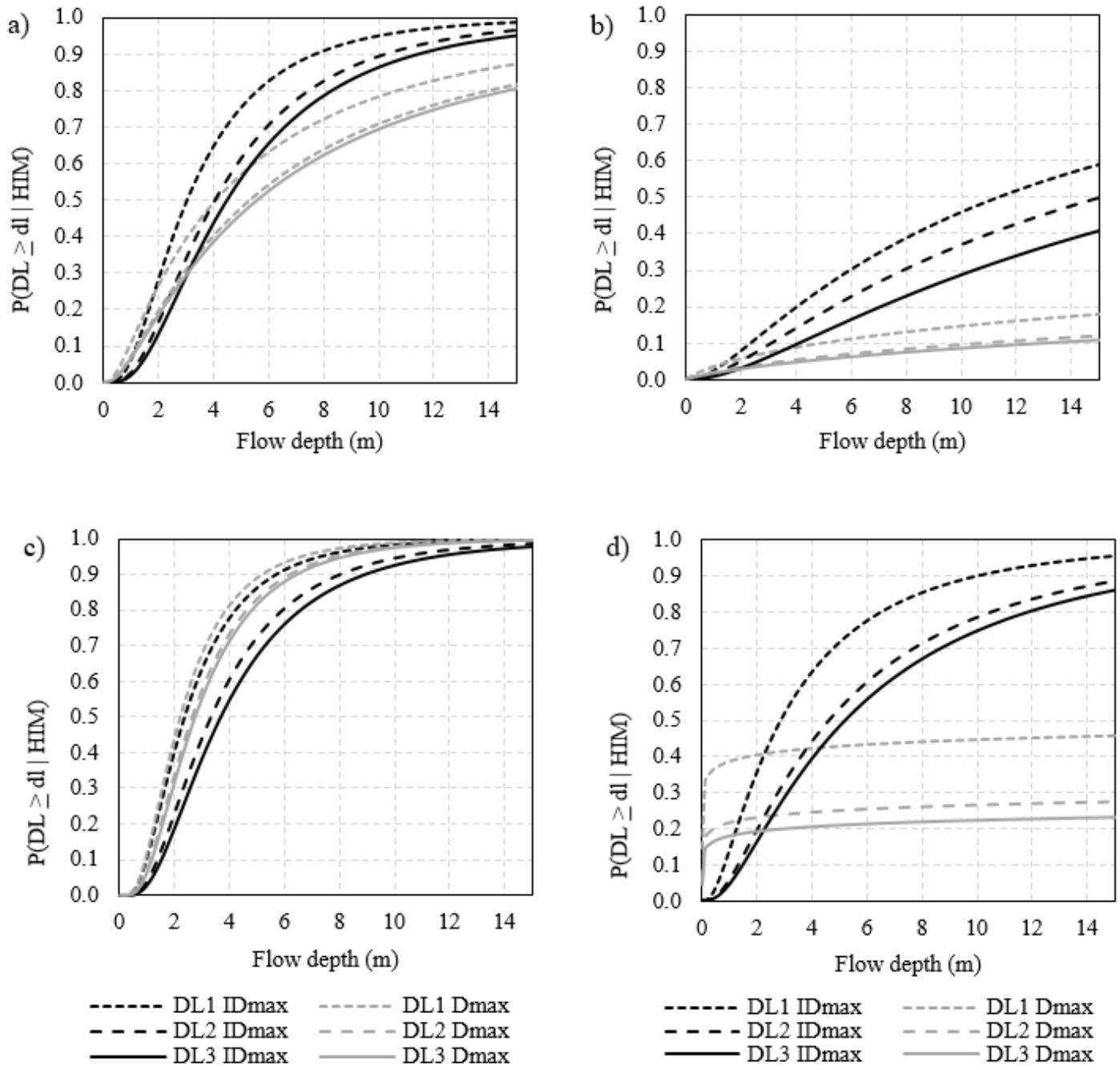

Figure 7

Tsunami fragility curves using IDmax and Dmax for mixed utility pole material (a) and concrete (b), steel (c), and timber (d) construction

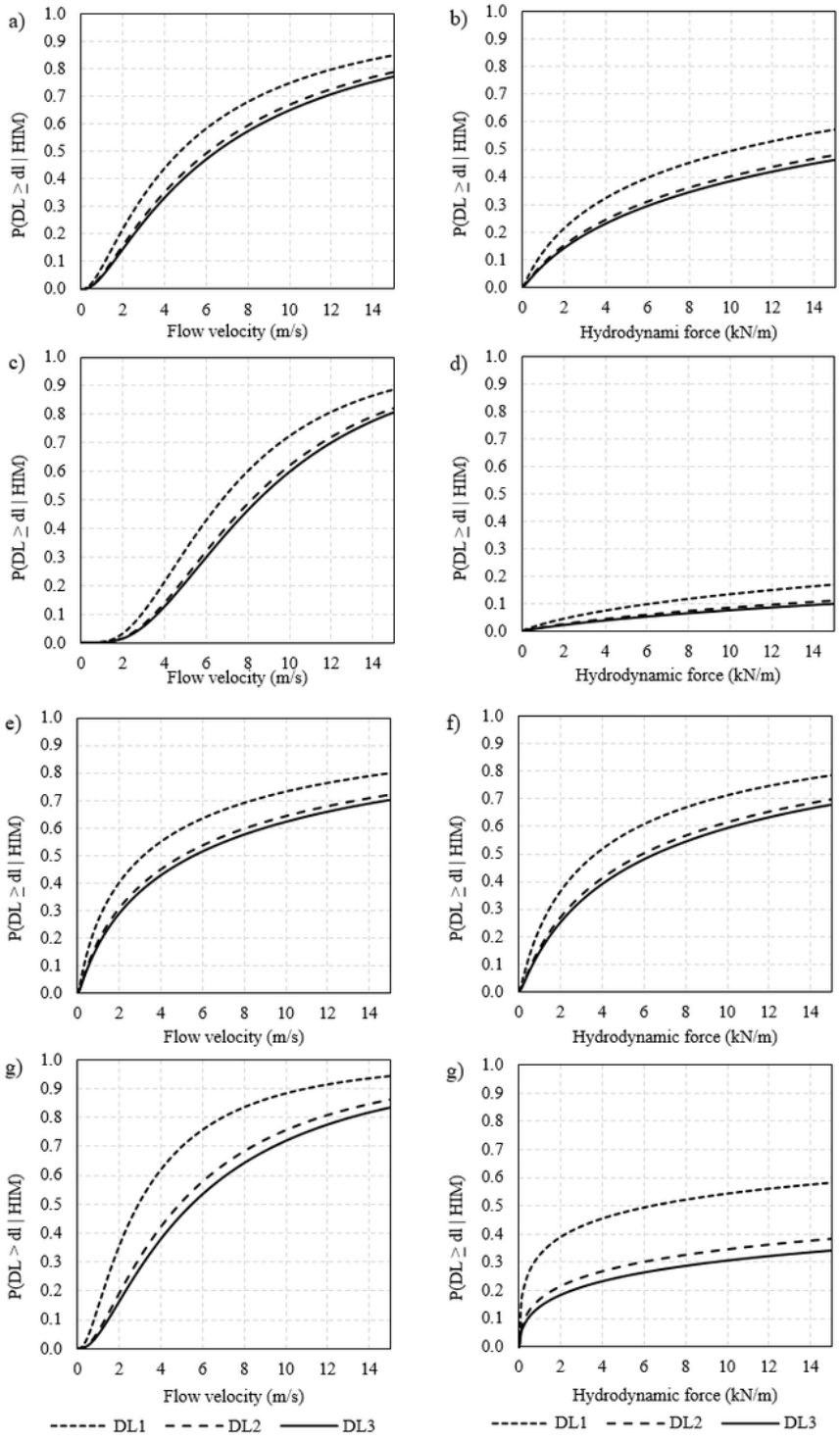

Figure 8

Tsunami fragility curves using Vmax and Fmax (left to right) for mixed utility pole material (a, b) and concrete (c, d), steel (e, f), and timber (g, h) construction

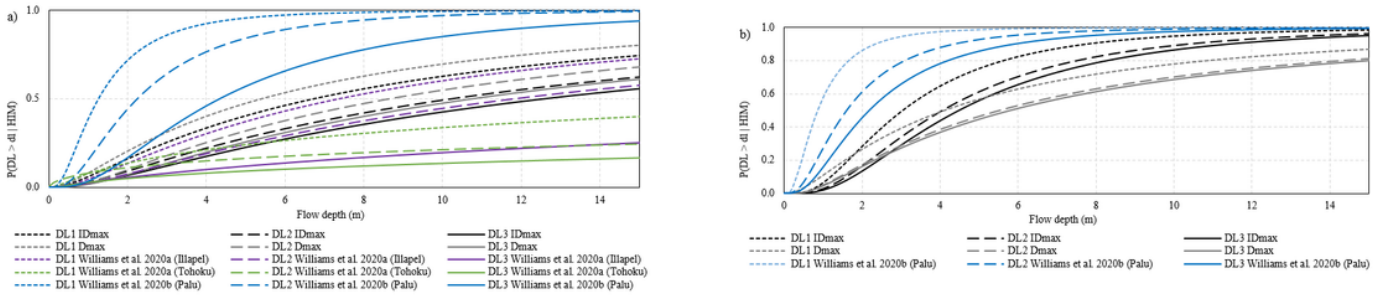

Figure 9

comparison with previous studies using flow depth as a HIM, for mixed construction (a) roads and (b) utility poles